

TRACE Analysis of the STS Target Flow Loop Conceptual Design



Aaron Wysocki
Belgacem Hizoum
Kevin Robb

June 2023



DOCUMENT AVAILABILITY

Reports produced after January 1, 1996, are generally available free via OSTI.GOV.

Website www.osti.gov

Reports produced before January 1, 1996, may be purchased by members of the public from the following source:

National Technical Information Service
5285 Port Royal Road
Springfield, VA 22161
Telephone 703-605-6000 (1-800-553-6847)
TDD 703-487-4639
Fax 703-605-6900
E-mail info@ntis.gov
Website <http://classic.ntis.gov/>

Reports are available to US Department of Energy (DOE) employees, DOE contractors, Energy Technology Data Exchange representatives, and International Nuclear Information System representatives from the following source:

Office of Scientific and Technical Information
PO Box 62
Oak Ridge, TN 37831
Telephone 865-576-8401
Fax 865-576-5728
E-mail reports@osti.gov
Website <https://www.osti.gov/>

This report was prepared as an account of work sponsored by an agency of the United States Government. Neither the United States Government nor any agency thereof, nor any of their employees, makes any warranty, express or implied, or assumes any legal liability or responsibility for the accuracy, completeness, or usefulness of any information, apparatus, product, or process disclosed, or represents that its use would not infringe privately owned rights. Reference herein to any specific commercial product, process, or service by trade name, trademark, manufacturer, or otherwise, does not necessarily constitute or imply its endorsement, recommendation, or favoring by the United States Government or any agency thereof. The views and opinions of authors expressed herein do not necessarily state or reflect those of the United States Government or any agency thereof.

Nuclear Energy and Fuel Cycle Division

**TRACE ANALYSIS OF THE STS NATURAL CIRCULATION FLOW LOOP
CONCEPTUAL DESIGN**

Aaron Wysocki
Belgacem Hizoum
Kevin Robb

June 2023

Prepared by
OAK RIDGE NATIONAL LABORATORY
Oak Ridge, TN 37831
managed by
UT-BATTELLE LLC
for the
US DEPARTMENT OF ENERGY
under contract DE-AC05-00OR22725

CONTENTS

LIST OF FIGURES	iv
LIST OF TABLES	v
ABSTRACT.....	1
1. MODEL DESCRIPTION	1
1.1 TRACE CAPABILITIES.....	1
1.1 GEOMETRY	2
1.1.1 Target Flow Channels	2
1.1.2 Target Solid Region	4
1.1.3 Riser and Downcomer.....	6
1.1.4 Pressurizer.....	10
1.1.5 Inner Annulus.....	11
1.1.6 Condenser Solid Region	12
1.1.7 Hydraulic Diameters	14
1.2 Material Properties.....	14
1.3 Operating Conditions	15
1.3.1 Inner Annulus.....	15
1.3.2 Target Energy Deposition	15
1.3.3 Initial Fluid Conditions	15
2. ANALYSIS RESULTS	16
2.1 RESULTS SUMMARY.....	16
2.2 RESULTS WITH NO PRESSURIZER	17
2.3 RESULTS WITH PRESSURIZER.....	20
2.4 RESULTS WITH BELLOWS	22
2.5 POSSIBLE ADDITIONAL DESIGN CHANGES TO CONSIDER.....	25
3. REFERENCES	27

LIST OF FIGURES

Figure 1. Diagram of the Second Target Station (STS) flow loop TRACE model.....	2
Figure 2. Numerical discretization of the TRACE target channels.....	3
Figure 3. Cross-cut drawing of the target and flow channels.	4
Figure 4. Depiction of the target solid region as modeled in TRACE.	4
Figure 5. Target solid geometry.	5
Figure 6. Energy deposition distribution used to determine the TRACE axial power factors.....	6
Figure 7. Numerical discretization of the lower riser section.	7
Figure 8. Numerical discretization of the upper riser section.	8
Figure 9. Numerical discretization of the upper volume connecting the riser to the downcomer.	8
Figure 10. Numerical discretization of the upper downcomer section.	9
Figure 11. Numerical discretization of the lower downcomer section.	10
Figure 12. Numerical discretization of the pressurizer.	11
Figure 13. Numerical discretization of the lower downcomer section.	12
Figure 14. Conceptual drawing of the condenser region.	13
Figure 15. Condenser solid region radial geometry.	14
Figure 16. Results with 84% initial liquid fraction, showing the target region pressure (top left), mass flow rate (top right), liquid temperature (bottom left), and peak tungsten temperature (bottom right).	18
Figure 17. Void fraction in the loop at a snapshot during the stable oscillations.	19
Figure 18. Final steady-state void fraction distribution in the pressurizer case with 97% initial liquid fraction.	20
Figure 19. Pressurizer case with 97% initial liquid, including the target region pressure (top left), mass flow rate (top right), liquid temperature (mid left), and peak tungsten temperature (mid right), and pressurizer liquid level (bottom).	21
Figure 20. Bellows case results at 2 MPa, including the target region pressure (top left), mass flow rate (top right), liquid temperature (bottom left), and peak tungsten temperature (bottom right).	23
Figure 21. Bellows case results at 1 MPa, including the target region pressure (top left), mass flow rate (top right), liquid temperature (bottom left), and peak tungsten temperature (bottom right).	24
Figure 22. Bellows case results at 1 MPa after adding riser-to-condenser heat transfer; shown are the target region pressure (top left), mass flow rate (top right), liquid temperature (bottom left), and peak tungsten temperature (bottom right).	25

LIST OF TABLES

Table 1. Relative power in each axial cell in the target	5
Table 2. Hydraulic diameters	14
Table 3. Material properties used in the TRACE model.....	15
Table 4. Summary of results (no riser-to-condenser heat transfer).....	16
Table 5. Summary of results (including riser-to-condenser heat transfer).....	16

ABSTRACT

This report documents the efforts to model the conceptual design of the Oak Ridge National Laboratory Second Target Station (STS) natural circulation flow loop using the U.S. Nuclear Regulatory Commission's TRACE code. The purpose of the STS is to provide a neutron source to advance materials research in a variety of fields. The natural circulation flow loop is one of the proposed designs for removing the heat generated within the STS tungsten target during operation.

The results, summarized in Section 2.1, support the conclusion that the conceptual STS natural circulation flow loop design provides sufficient cooling of the tungsten target and exhibits predictable flow behavior, provided that certain design features and/or operating conditions are used. In particular, they are as follows:

- A sufficient initial liquid volume fraction is required to avoid dryout of the target flow channels.
- Inclusion of a pressurizer or bellows volume at the top of the loop is recommended and is capable of achieving steady, non-oscillatory flow and temperature conditions at sufficiently high loop pressure.

Section 1 provides a detailed description of the geometry and assumptions used in the model, and Section 2 presents the results for the current flow loop design as well as some investigation of potential design modifications with the goal of enhancing the thermal hydraulic stability of the loop.

1. MODEL DESCRIPTION

1.1 TRACE CAPABILITIES

The thermal hydraulic systems code TRACE [1] has been widely applied for the modeling of various nuclear and non-nuclear flow and heat transfer systems. It is designed to perform best-estimate analyses of steady-state and transient scenarios across a broad range of operating conditions.

Features of TRACE relevant to this study include the following:

- Two-fluid, six-conservation-equation solution formulation (i.e., independent mass, momentum, and energy conservation for each phase)
- Second-order spatial numerical method, giving optimum accuracy for stability calculations
- Temperature- and pressure-dependent fluid thermophysical properties calculated from built-in steam tables
- All heat transfer coefficients, wall friction factors, and liquid–vapor interface terms calculated from built-in correlations
 - Accounts for various single-phase flow regimes (i.e., laminar and turbulent) and two-phase flow regimes (i.e., bubbly, slug, annular mist)
 - Similar accounting for heat transfer regimes, including single- and two-phase as well as pre- and post-critical heat flux
- Material properties supplied (in this case) by user-defined tables

TRACE has been developed and validated against a broad set of single-effects tests and integral experimental tests covering a wide range of single- and two-phase flow and heat transfer phenomena. The code has been used extensively for reactor applications as well as for modeling a variety of experimental flow loops.

Moreover, TRACE has been used frequently in the analysis of thermal hydraulic instabilities, which is particularly relevant for this study. This use includes validation of TRACE against real-world instability data in experimental flow loops [2] and operating boiling water reactors [3, 4]. TRACE has been successful in reproducing the measured flow instabilities and has demonstrated accuracy on par with or better than that of other available tools.

1.2 GEOMETRY

A diagram of the Oak Ridge National Laboratory Second Target Station (STS) flow loop TRACE model is shown in Figure 1. Initial studies (Section 2) were performed without the pressurizer component and with only the upper downcomer pipe connected to the condenser for heat removal. Additional studies considered the inclusion of the pressurizer as well as taking credit for heat removal from the upper riser region, as indicated in the figure.

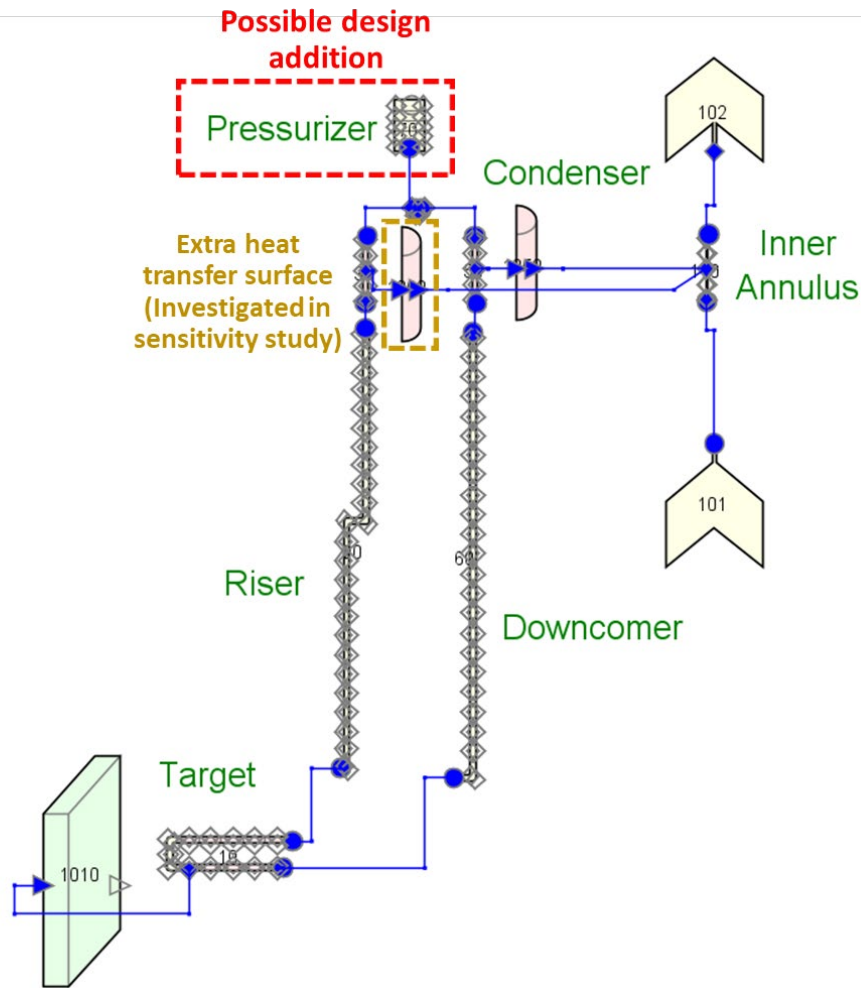


Figure 1. Diagram of the Second Target Station (STS) flow loop TRACE model.

1.2.1 Target Flow Channels

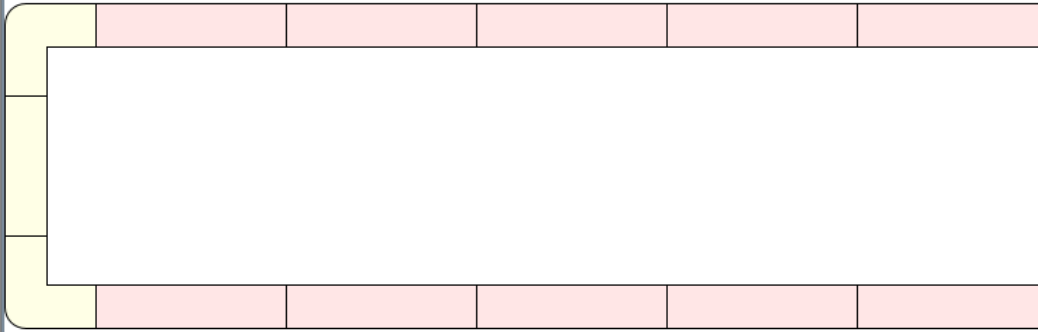
Figure 2 shows the geometric configuration of the TRACE target channel control volumes. Cell number 1 is the cell at the inlet of the target. The “Length” column gives the full length of each control volume, whereas the “DZ” column gives the change in elevation across the control volume. For example, when

modeling elbow cells, TRACE assumes that half the cell is horizontal and half is vertical, which explains the “DZ” values shown. The two elbow cells were included to account approximately for the form losses in the semicircular bend of the physical channels. Their cell lengths were chosen to preserve the true elevation gain of 0.068 m from the provided drawings.

Note that the flow area and cell volumes shown here are for a single target channel; a multiplier of 11 is applied to this component in the TRACE model to simulate all 11 physical channels in the target. This multiplier scales the effective flow area and volume of each cell without changing the hydraulic diameter ($3.04414\text{E-}3\text{ m}$).

These 11 physical channels include the 7 channels beneath the target and the 2 channels on each side of the target, as shown in Figure 3. These 11 channels on the bottom half of the target region turn upward and return along the top half of the target region; although in reality the side channels may have slightly shorter flow lengths and less elevation change than the bottom/top channels, the TRACE model more simply treats all 11 channels as if they were top/bottom channels.

Geometry - Pipe 10



Row Order: Automatic

Cell Number	Volume (m ³)	Length (m)	Vol. Avg. Flow Area (m ²)	DZ (m)	2D Drawing Pivot
13	1.268072E-6	0.0548	2.314E-5	0.0	<input type="checkbox"/>
12	1.268072E-6	0.0548	2.314E-5	0.0	<input type="checkbox"/>
11	1.268072E-6	0.0548	2.314E-5	0.0	<input type="checkbox"/>
10	1.268072E-6	0.0548	2.314E-5	0.0	<input type="checkbox"/>
9	1.268072E-6	0.0548	2.314E-5	0.0	<input type="checkbox"/>
8	7.8676E-7	0.034	2.314E-5	0.017	<input checked="" type="checkbox"/>
7	7.8676E-7	0.034	2.314E-5	0.034	<input type="checkbox"/>
6	7.8676E-7	0.034	2.314E-5	0.017	<input type="checkbox"/>
5	1.268072E-6	0.0548	2.314E-5	0.0	<input type="checkbox"/>
4	1.268072E-6	0.0548	2.314E-5	0.0	<input type="checkbox"/>
3	1.268072E-6	0.0548	2.314E-5	0.0	<input type="checkbox"/>
2	1.268072E-6	0.0548	2.314E-5	0.0	<input type="checkbox"/>
1	1.268072E-6	0.0548	2.314E-5	0.0	<input type="checkbox"/>
Total	1.5041E-5	0.65	3.0082E-4	0.068	

Figure 2. Numerical discretization of the TRACE target channels.

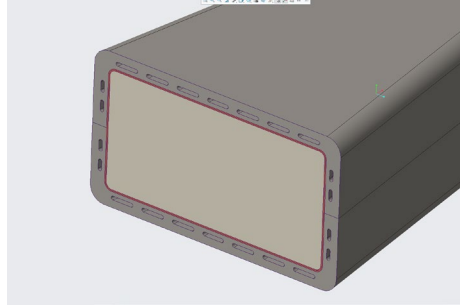


Figure 3. Cross-cut drawing of the target and flow channels.

1.2.2 Target Solid Region

The target solid region is modeled as a 2D slab, as depicted in Figure 4. This includes axial dependence (along the length of the flow channels) as well as depth through the tungsten and other materials. The TRACE model performs a 2D time-dependent heat conduction calculation in these two dimensions, based on the supplied power distribution (discussed below) and material properties (Section 1.2). In the physical system, there are 4 side channels that cool the lateral faces of the target, and the remaining 7 channels cool the bottom and top faces of the target (Figure 3). However, the TRACE model makes the simplifying assumption that all 11 channels are located along the top and bottom faces of the target, such that no temperature gradients in the lateral third dimension are modeled. In other words, all 11 channels are effectively contributing to the cooling but without requiring a full 3D conduction calculation, which TRACE does not support.

The target solid region is divided into 5 uniform axial cells, each 0.0548 m in length, corresponding to the cell lengths used in the adjacent fluid channels. This 0.274 m total target length does not include the semicircular rounded region on the outer tip of the target (Figure 4). This rounded region, and the additional heat transfer length along the curved portion of the channels, is ignored in the TRACE model, due to the difficulty of modeling this in the 2D slab geometry. This reduction in the total heat transfer surface area is slightly conservative, in terms of overpredicting the average tungsten temperature.

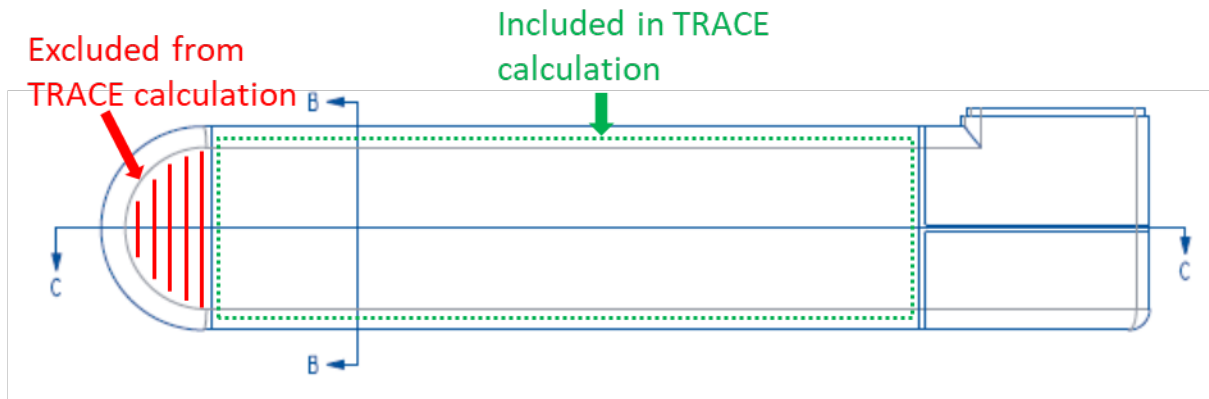


Figure 4. Depiction of the target solid region as modeled in TRACE.

Figure 5 shows the numerical discretization as a function of depth into the slab. Note that although TRACE labels the material boundaries here as “radii,” these actually refer to the depth in Cartesian coordinates in this case. The outer surfaces of the Inconel-718 regions are connected to the target fluid channels so as to provide solid-to-coolant convective heat transfer out of both the bottom and top edges of the target solid region.

Define Radial Geometry

Mesh Options

☐ Standard Mesh
 ☒ Finite Element
 ☐ Lumped Parameter

Material Regions Add Remove

Material	Inner Radius (m)	Outer Radius (m)	Thickness (m)	Calculation	Node Count	Start Node (m)
Material 52 (Inconel718)	0.0	2.0E-3	2.0E-3	Manual	3	
Material 51 (Copper)	2.0E-3	3.0E-3	1.0E-3	Manual	3	
Material 50 (Tungsten)	3.0E-3	0.063	0.06	Manual	5	
Material 51 (Copper)	0.063	0.064	1.0E-3	Manual	3	
Material 52 (Inconel718)	0.064	0.066	2.0E-3	Manual	3	

Radial Intervals Split Merge

Interval Number	Material	Inner Radius (m)	Outer Radius (m)	Relative Inside (-)	Relative Outside (-)	Thickness (m)
1	Material 52 (Inconel718)	0.0	2.0E-3	0.0	0.03030303	2.0E-3
2	Material 51 (Copper)	2.0E-3	3.0E-3	0.03030303	0.045454545	1.0E-3
3	Material 50 (Tungsten)	3.0E-3	0.033	0.045454545	0.5	0.03
4	Material 50 (Tungsten)	0.033	0.063	0.5	0.95454545	0.03
5	Material 51 (Copper)	0.063	0.064	0.95454545	0.96969697	1.0E-3
6	Material 52 (Inconel718)	0.064	0.066	0.96969697	1.0	2.0E-3

Help
OK
Cancel

Figure 5. Target solid geometry.

Table 1 shows the axial power distribution used in the tungsten. An axial position of 0 m corresponds to the left edge of the green region in Figure 4. The power factors were calculated by analytically integrating the polynomial energy deposition distribution depicted in Figure 6 and normalizing to an average of 1.0 for the five axial regions. At the time of this calculation, it was unknown whether the curve in Figure 6 accounts for the length of the rounded tungsten section; however, the normalization of the power factors ensured that the total tungsten power was exactly 20 kW, so any possible power shape discrepancies would be minor and would not appreciably impact the results.

Table 1. Relative power in each axial cell in the target

Axial interval start (m)	Axial interval stop (m)	Axial interval midpoint (m)	Normalized power factor
0.0000	0.0548	0.0274	1.930
0.0548	0.1096	0.0822	1.291
0.1096	0.1644	0.1370	0.810
0.1644	0.2192	0.1918	0.541
0.2192	0.2740	0.2466	0.427

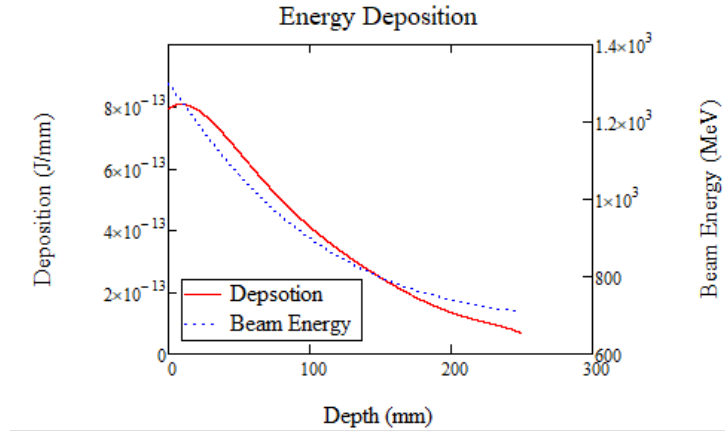


Figure 6. Energy deposition distribution used to determine the TRACE axial power factors.

1.2.3 Riser and Downcomer

The 5.25 m vertical span of the riser was split into two sections: a lower 4.5 m section and an upper 0.75 m section. This split has no impact on the solution and was done for convenience so as to more clearly demarcate where the condenser region (upper 0.75 m) began. The downcomer was split in the same manner.

Figures 7 through 11 show the numerical discretization of the riser and downcomer sections. Elbow cells were used at the riser inlet and downcomer outlet to properly connect to the horizontal cells of the target channel and provide some treatment of form losses. Additional elbows were modeled partway up the riser, representing the 90° bends in the real system. The elbow cells and remaining cells were sized to give 4.5 m total elevation gain in the lower riser section (4.568 in the lower downcomer, accounting for the extra 0.068 m elevation change in the target channels) while generally attempting to keep the length of the computational cells to 0.2 m or less. This cell spacing was chosen based on engineering judgment to provide sufficiently accurate results for this conceptual design study.

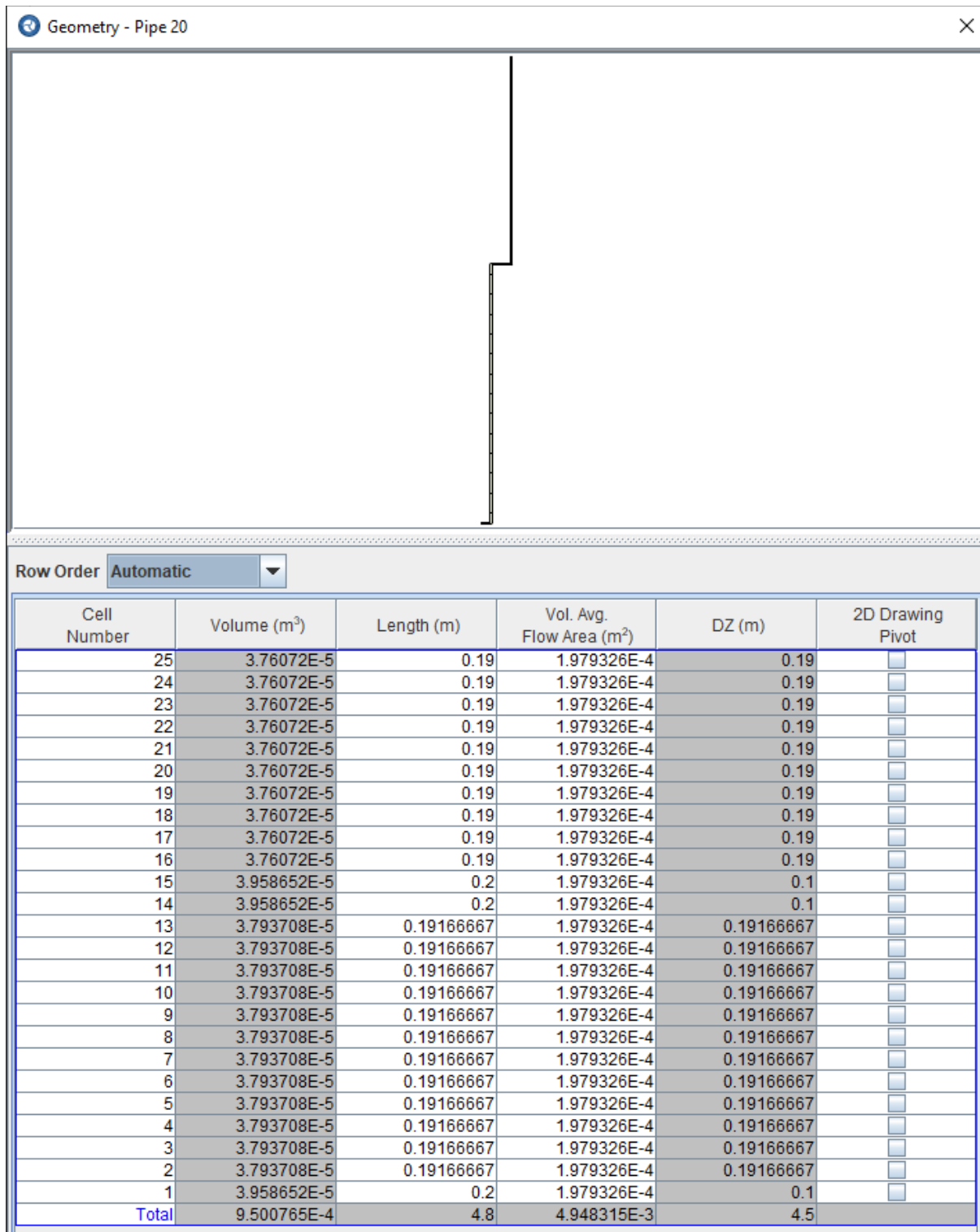


Figure 7. Numerical discretization of the lower riser section.

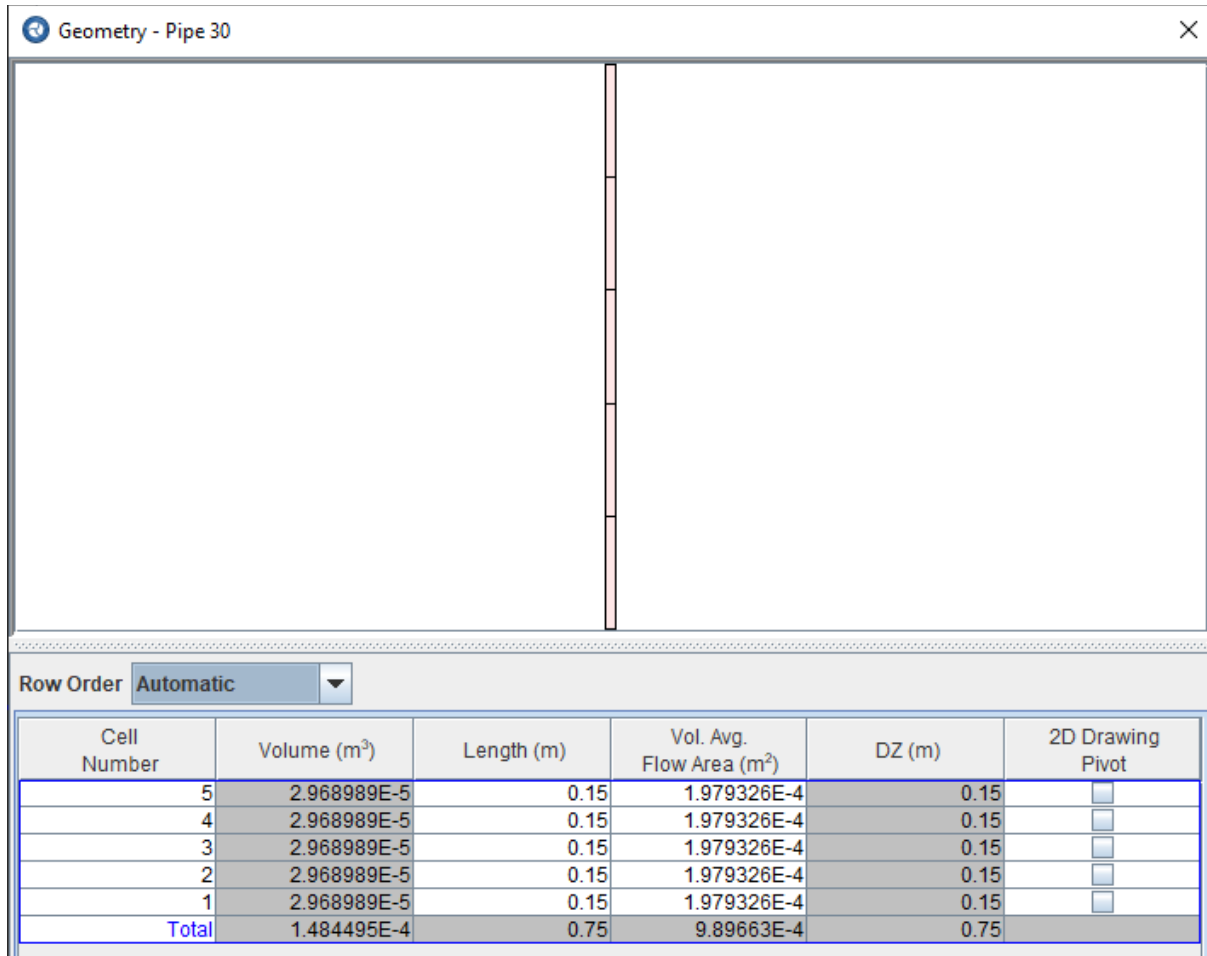


Figure 8. Numerical discretization of the upper riser section.

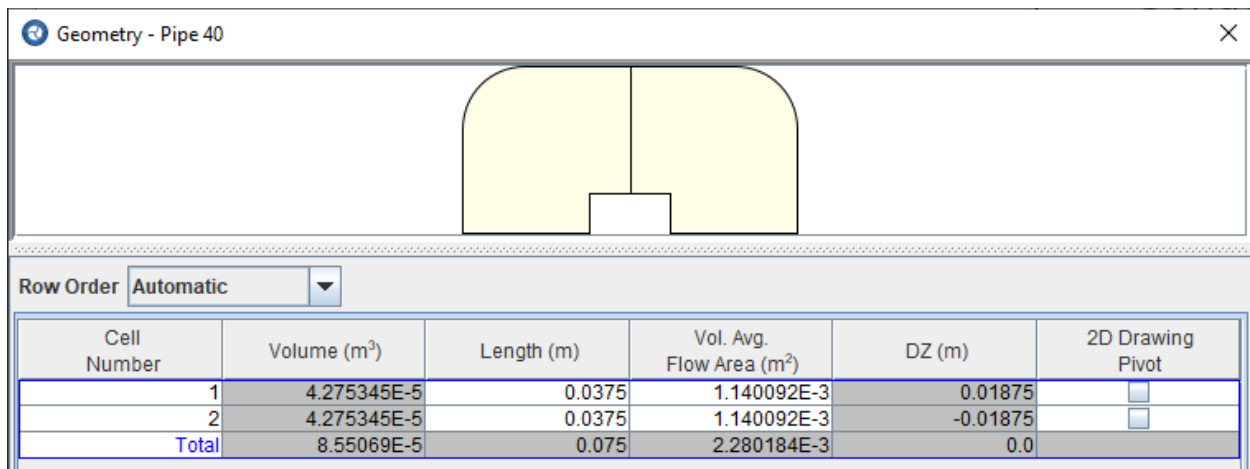


Figure 9. Numerical discretization of the upper volume connecting the riser to the downcomer.

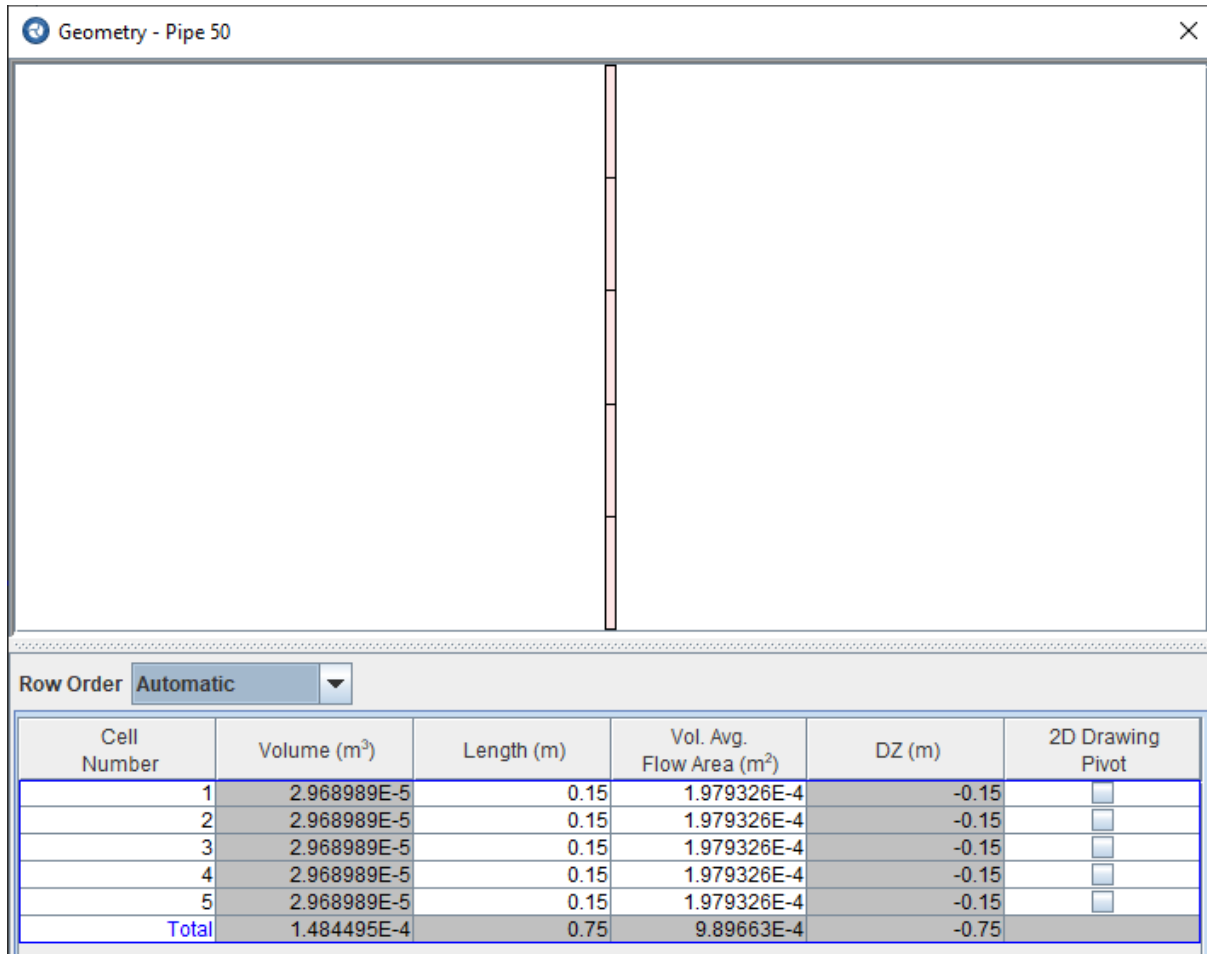


Figure 10. Numerical discretization of the upper downcomer section.

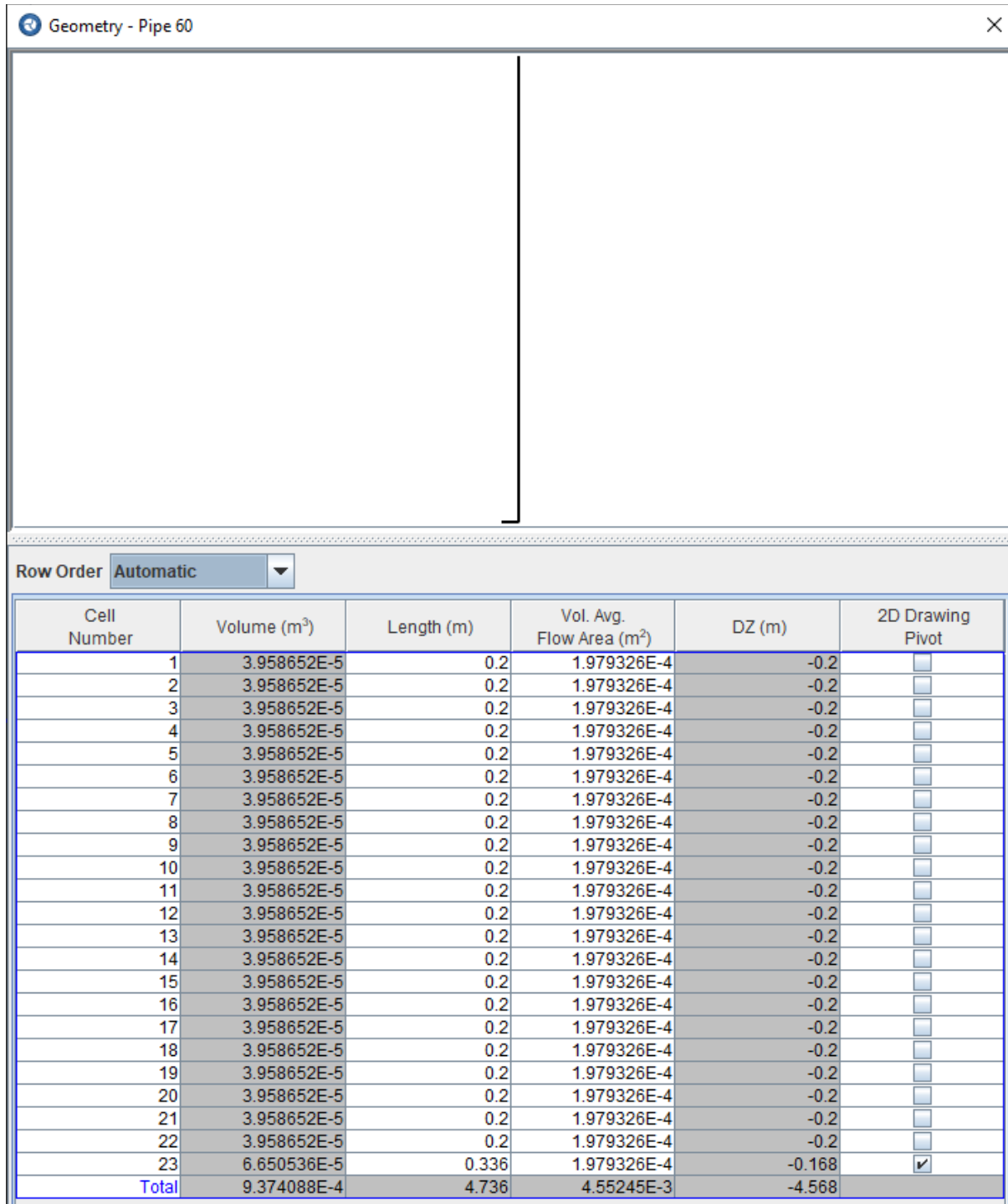


Figure 11. Numerical discretization of the lower downcomer section.

1.2.4 Pressurizer

The pressurizer, used in some of the analyses, was modeled as a separate component in TRACE for convenience. However, in practice, it could be implemented in the design by simply expanding the upper

connector region between the riser and downcomer, the goal being to allow a stationary vapor “bubble” to remain at the top of the pressurizer volume without being swept downward by the main flow in the loop.

Geometry values selected for this study are given in Figure 12. The total pressurizer volume (i.e., $1.173\text{E-}3 \text{ m}^3$) was chosen as half of the volume of the remaining loop ($2.346\text{E-}3 \text{ m}^3$), as a somewhat arbitrary but seemingly reasonable starting point. It is possible that a smaller pressurizer could perform suitably well instead, but the impact of pressurizer volume on loop performance has not yet been studied.

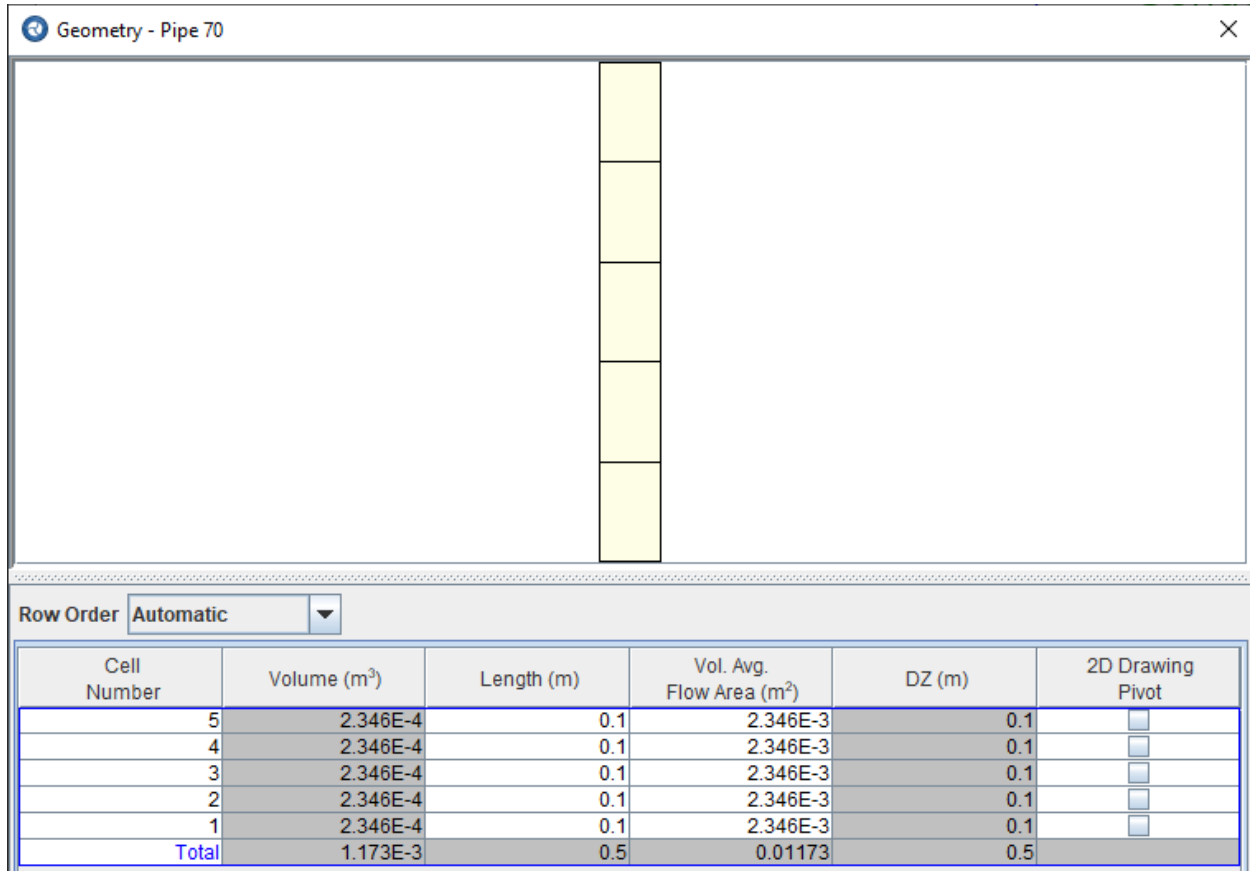


Figure 12. Numerical discretization of the pressurizer.

1.2.5 Inner Annulus

The inner annulus (i.e., condenser) flow region was discretized as shown in Figure 13.

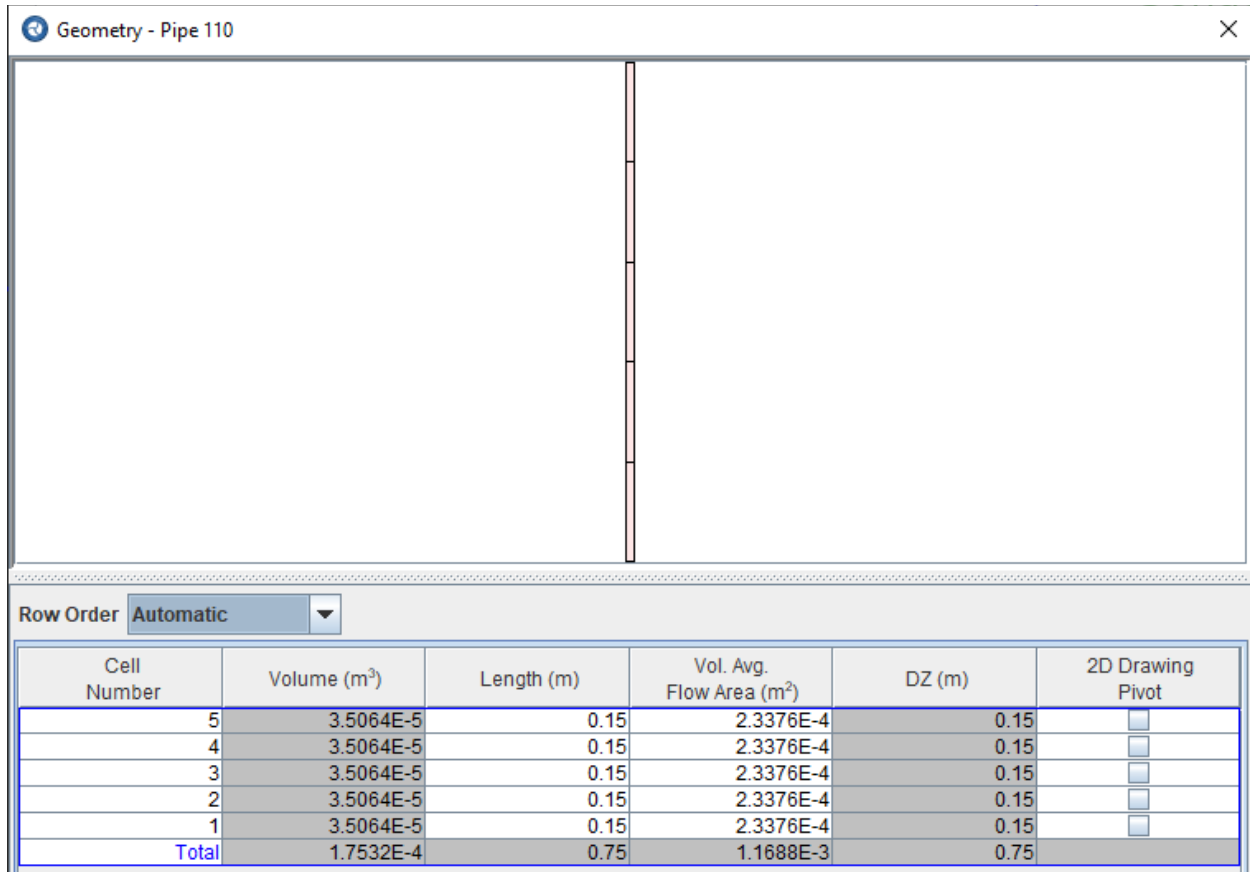


Figure 13. Numerical discretization of the lower downcomer section.

1.2.6 Condenser Solid Region

A top-down conceptual drawing of the condenser and inner annulus geometry was provided for this work and is shown in Figure 14. The red region in the figure is the downcomer flow channel. The thickness of the aluminum between the downcomer and inner annulus is 0.75 in. (0.019 m). The riser flow channel is not shown in the figure, but it will be drilled into the same billet as the downcomer, with a distance to the inner annulus of greater than 0.75 in. Also not shown is the remainder of the billet and surrounding structures, which may have some impact on heat conduction as well.

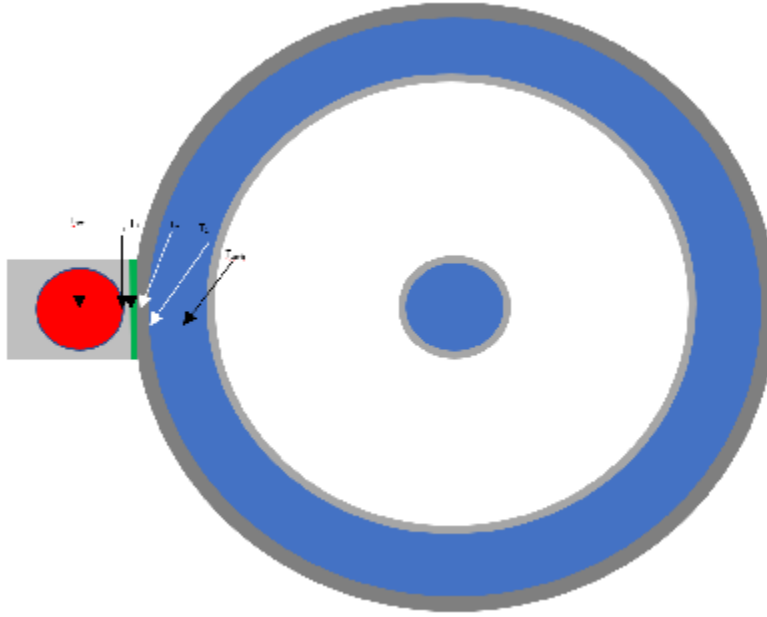


Figure 14. Conceptual drawing of the condenser region.

One of two geometric options could have been chosen in TRACE to model the solid condenser region. It could have been modeled as a 2D slab (axial- and “radial”-dependent) with the downcomer on one side and the inner annulus on the other side. Alternatively, it could have been modeled as a 2D cylindrical shell with the downcomer on the interior of the cylindrical shell and the secondary inner annulus flow modeled as the exterior of the cylindrical shell.

Neither approach is fully representative of the geometry shown in Figure 14. Ideally, a 2D or 3D finite element code such as COMSOL or STAR-CCM+ would be used to model the exact geometry and accurately calculate the effective thermal conductance between the two flow regions under representative operating conditions, which could then be used to tune the TRACE geometric representation and/or apply appropriate scaling multipliers to the TRACE heat transfer coefficients, to match the COMSOL predictions.

However, for the current work, the condenser geometry was approximated with the 2D cylindrical shell approach. An axial condenser length of 0.75 m was used, split into five cells of 0.15 m each and connected to the uppermost five cells of the downcomer. The radial geometry of the condenser solid region is shown in Figure 15. The inner radius was set to the true radius of the downcomer channel; this was done to preserve the correct heated perimeter in that region. A shell thickness of 0.019 m was used, matching the closest distance between the downcomer and inner annulus in the real system. The largest room for error in this method is in the way the heated perimeter of the secondary annulus is represented. The current TRACE model sets this to the circumference of the outer shell (with radius of 0.027 m). Additional work could be done to examine the acceptability of this approach. Note, however, that most results in this report only model the heat transfer from the downcomer to the secondary side, ignoring any additional heat transfer from the riser.

Define Radial Geometry

Mesh Options

☐ Standard Mesh
 ☒ Finite Element
 ☐ Lumped Parameter

Material Regions Add Remove

Material	Inner Radius (m)	Outer Radius (m)	Thickness (m)	Calculation	Node Count	Start Node (m)
Material 53 (Aluminum)	7.9375E-3	0.0269875	0.01905	Manual	5	

Radial Intervals Split Merge

Interval Number	Material	Inner Radius (m)	Outer Radius (m)	Relative Inside (-)	Relative Outside (-)	Thickness (m)
1	Material 53 (Aluminum)	7.9375E-3	0.0174625	0.0	0.5	9.525E-3
2	Material 53 (Aluminum)	0.0174625	0.0269875	0.5	1.0	9.525E-3

Help OK Cancel

Figure 15. Condenser solid region radial geometry.

1.2.7 Hydraulic Diameters

Hydraulic diameters for each region are shown in Table 2.

Table 2. Hydraulic diameters

Component	Hydraulic diameter (m)
Target channels	0.003044
Riser (both sections)	0.015875
Upper connector	0.038100
Downcomer (both sections)	0.038100
Inner annulus	0.006350

1.3 MATERIAL PROPERTIES

The target and condenser materials were assigned constant (i.e., non–temperature-dependent) values, as shown in Table 3, roughly corresponding to the temperatures observed for this problem (roughly 650 K or less).

Table 3. Material properties used in the TRACE model.

	Tungsten	Copper	Inconel-718	Aluminum
Specific Heat (J/kg · K)	130 [5]	390 [5]	435 [6]	910 [5]
Density (kg/m³)	19600 [7]	8940 [7]	8190 [6]	2712 [7]
Conductivity (W/m · K)	84 *	392 [8]	11.4 [6]	240 [8]

* Tungsten conductivity of 84 W/m · K was provided specifically for STS

A surface roughness of 2 microns was used for all fluid surfaces in the model, which impacts the friction factors calculated internally by TRACE.

1.4 OPERATING CONDITIONS

1.4.1 Inner Annulus

A fixed inlet flow rate of 0.449 kg/s, inlet temperature of 35 °C, and outlet pressure of 101.3 kPa were used for the inner annulus channel.

1.4.2 Target Energy Deposition

Although a time-dependent energy deposition is applied to the target in reality, the TRACE model assumes a fixed, steady 20 kW power deposition in the target—or 10 kW for some sensitivity studies—for the full duration of the simulation.

In the real system, some beam energy is deposited directly in the coolant; this deposition was ignored in the current TRACE calculation, although TRACE is capable of modeling it in the future if desired. In the present calculation, the full beam energy deposition is applied to the target itself.

1.4.3 Initial Fluid Conditions

Initial conditions of 101.3 kPa and 100 °C were set throughout the primary loop. Initial vapor void fractions were adjusted on a case-by-case basis to adjust the initial loop-averaged liquid volume fraction—or, relatedly, the initial mass charge of water in the loop—in each simulation. For example, an initial 84% liquid volume was achieved by setting an initial 100% vapor void fraction in the top 0.75 m of the riser and downcomer, 100% void fraction in the upper connector region, and 0% void everywhere else. Lower initial liquid volumes were achieved by setting additional riser and downcomer cells to 100% void at decreasing elevations.

2. ANALYSIS RESULTS

2.1 RESULTS SUMMARY

The main results obtained in this study are summarized in Table 4 and Table 5. Results are given both with and without riser-to-condenser heat transfer. Downcomer-to-condenser heat transfer is always included. This is intended to encapsulate uncertainties in how the condenser region is modeled and to highlight the degree to which the condenser design impacts the loop performance.

With no pressurizer or bellows, the two-phase natural circulation flow was found to be oscillatory in all cases. For initial liquid volume fractions of at least 50%, acceptable tungsten temperatures were observed (i.e., 620 K or less) with very small temperature fluctuation even in the presence of flow oscillations. The fluid temperature and pressure oscillations could pose long-term issues in terms of cycling and fatigue; future analysis would be needed to understand their impact and, if necessary, to mitigate the consequences through design changes.

The TRACE analyses show that, alternatively, oscillations can be avoided by including either a pressurizer volume or bellows. Non-oscillatory, single-phase natural circulation conditions were achieved with sufficiently high loop pressure: 0.6 or 1.8 MPa, depending on the condenser heat transfer modeling assumption. The pressurizer and bellows approaches were found to be essentially equivalent from a loop thermal and flow perspective, provided that they are capable of facilitating the loop pressure levels mentioned above.

Table 4. Summary of results (no riser-to-condenser heat transfer)

Pressurizer Type	Initial Liquid Frac.	Steady State Results		
		Tungsten Hotspot Temperature	Fluid Temperature (Target Outlet)	Loop Pressure
No Pressurizer	84%	620 K	388 ± 20 K	1.25 ± 0.5 MPa
	50%	600 K	450 ± 25 K	0.6 ± 0.5 MPa
	20%	2600 K	425 ± 25 K	0.5 ± 0.25 MPa
Pressurizer	97%	645 K	477 ± 5 K	1.9 ± 0.05 MPa
Bellows	100%	648 K	480 K	2 MPa

Table 5. Summary of results (including riser-to-condenser heat transfer)

Pressurizer Type	Initial Liquid Frac.	Steady State Results		
		Tungsten Hotspot Temperature	Fluid Temperature (Target Outlet)	Loop Pressure
No Pressurizer	84%	592 K	400 ± 30 K	0.6 ± 0.4 MPa
Bellows	100%	625 K	428 K	1 MPa

The following sections provide the detailed results supporting the conclusions given above.

2.2 RESULTS WITH NO PRESSURIZER

For the current STS flow loop design with no added pressurizer volume, cases were run with several different initial liquid fractions: 20%, 50%, 84%, and 95% (as a fraction of the total loop volume). The initial fluid pressure was 101.3 kPa. Each case was run at 20 kW power.

The 20%, 50%, and 84% initial liquid cases were predicted to be oscillatory. Results for the 84% initial liquid case are shown in Figure 16 and Figure 17. The flow exhibits behavior consistent with density-wave oscillations, in which low-density (high void fraction) “waves” travel throughout the loop in a periodic fashion. Similar behavior has been observed in real-world two-phase natural circulation flow loops and in operating boiling water reactors. This type of instability is caused by complex interactions among flow rate, frictional and gravitational pressure drop, and convective/boiling heat transfer.

Additional no-pressurizer cases were run that included riser-to-condenser heat transfer (i.e., instead of downcomer-to-condenser only). The results were unstable in a similar fashion, although typically at lower pressure. For example, with 84% initial liquid, the final oscillatory pressure level fluctuated between ~0.2 to 1.0 MPa, compared to ~0.7 to 1.8 MPa in Figure 16.

Although design changes could potentially lead to non-oscillatory conditions in the current two-phase (no-pressurizer) configuration, the most reliable way to avoid oscillations in this loop was found to be the inclusion of a pressurizer or bellows volume and allowing for single-phase oscillation conditions, as shown in subsequent sections.

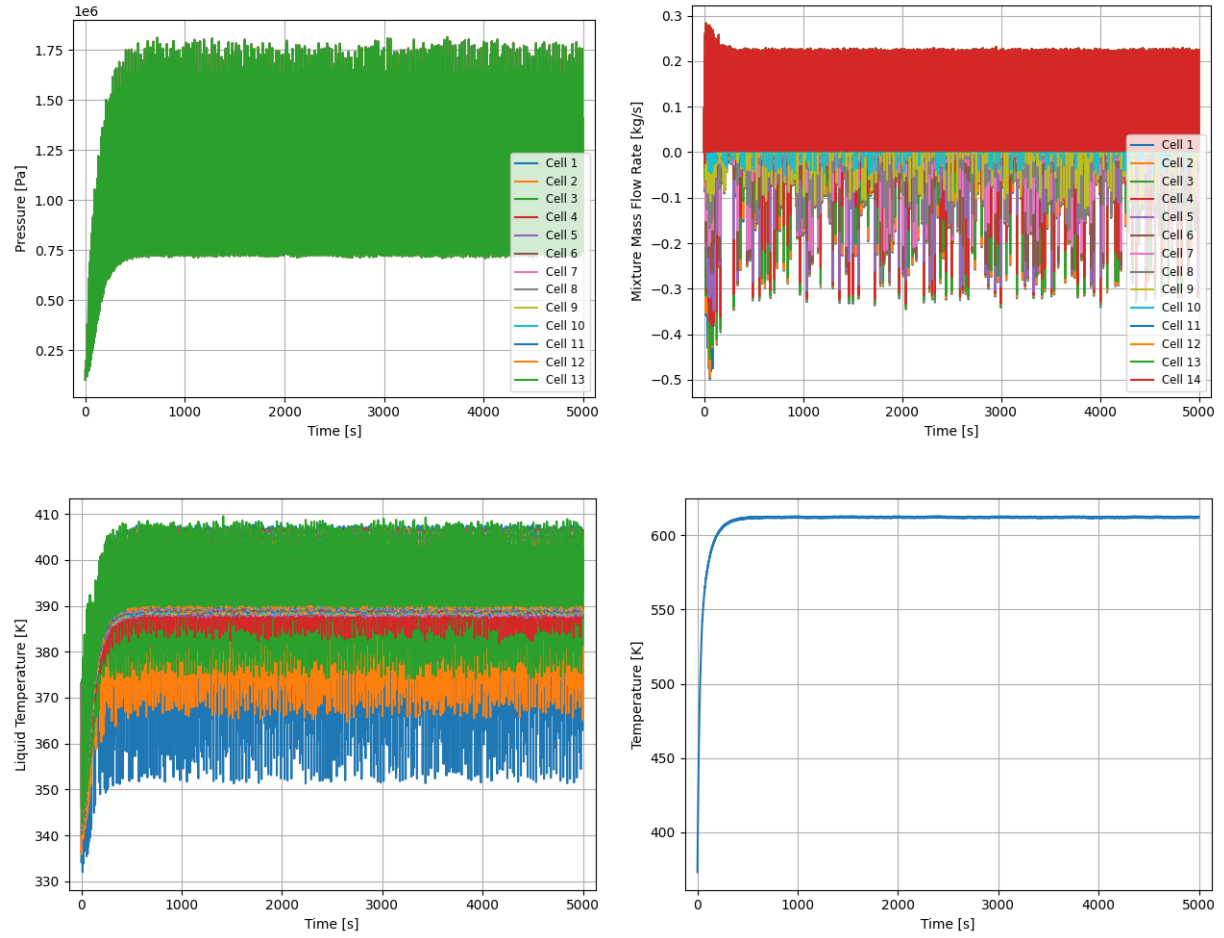


Figure 16. Results with 84% initial liquid fraction, showing the pressure (top left), mass flow rate (top right), and liquid temperature (bottom left) in the target region cells, and peak tungsten temperature in the target (bottom right).

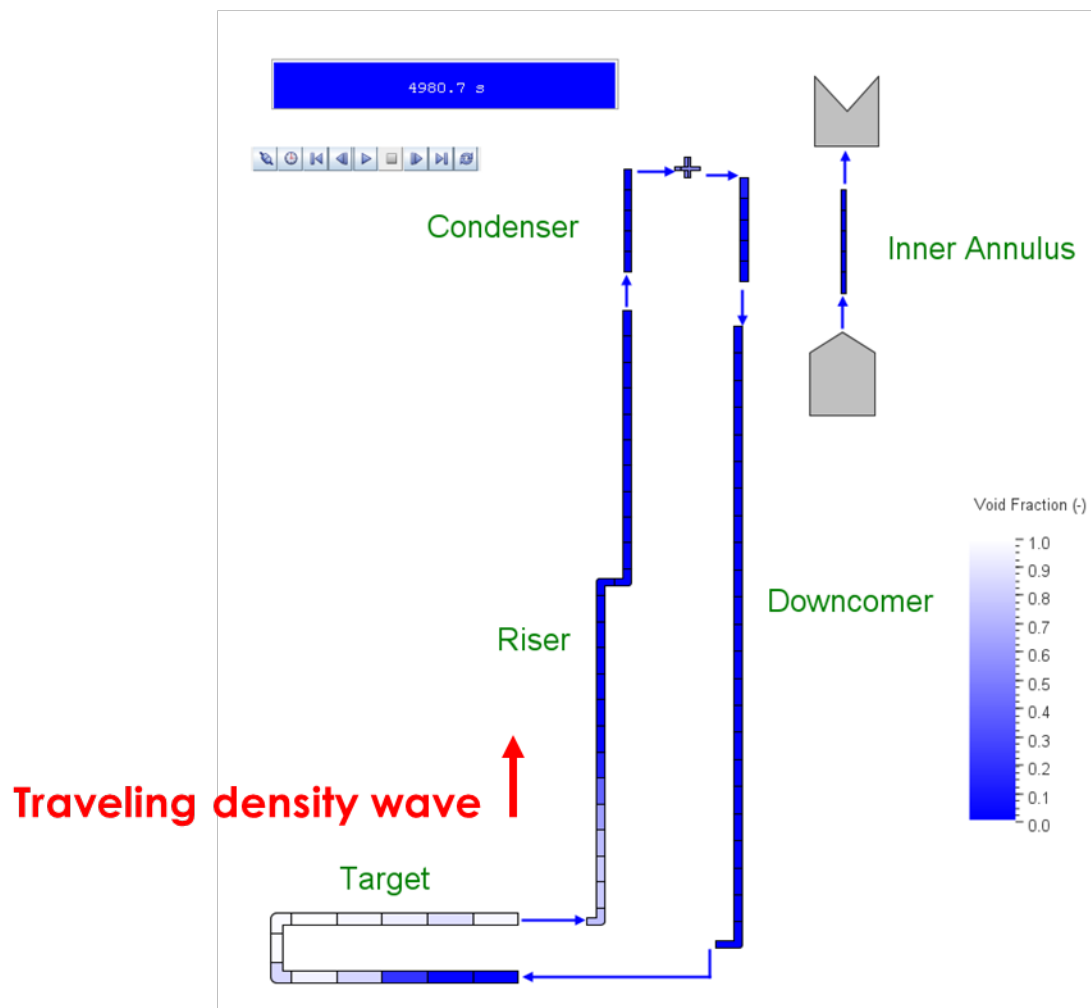


Figure 17. Void fraction in the loop at a snapshot during the stable oscillations.

2.3 RESULTS WITH PRESSURIZER

An additional study was performed to examine the impact of adding a pressurizer volume, the geometry of which is described in Section 1.1.4. The pressurizer volume of $1.173\text{E-}3\text{ m}^3$ —that is, 50% of the volume of the remainder of the loop—was somewhat arbitrarily chosen; further study could be done to determine whether a smaller pressurizer volume would be sufficient instead.

Cases were run at various initial liquid fractions. The most stable cases were obtained with very high initial liquid fractions, such as the 97% initial liquid case shown in Figure 18 and Figure 19. The reason is because single-phase natural circulation flow is the most stable flow configuration, but this single-phase flow condition was achieved only at quite high pressure levels ($\sim 2\text{ MPa}$): this pressure is a function of the condenser heat transfer capacity, as shown in Section 2.4. At lower pressures, or when using lower initial liquid volume, boiling occurred within the loop and promoted less stable behavior. Note that even though the initial liquid fraction was very high (i.e., an initial liquid level of 0.45 m in the 0.5 m pressurizer), the amount of liquid actually decreased as the loop heated up, resulting in a reduction of the pressurizer liquid level down to $\sim 0.3\text{ m}$ at steady state.

It is possible that changing the size of the pressurizer could lessen the required initial liquid fraction, but that effect has not yet been studied. Also, it is important to note that the condenser heat transfer capacity has a strong effect on the pressure, and presumably the initial liquid fraction, required for single-phase natural circulation. This effect is demonstrated in the next section with the “Bellows” approach, due to the greater simplicity of modeling compared to that of the pressurizer case.

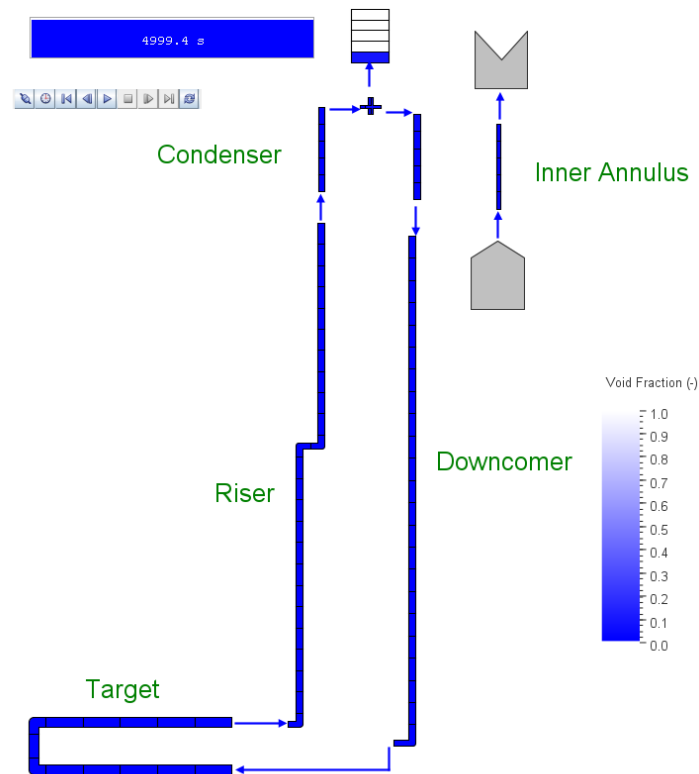


Figure 18. Final steady-state void fraction distribution in the pressurizer case with 97% initial liquid fraction.

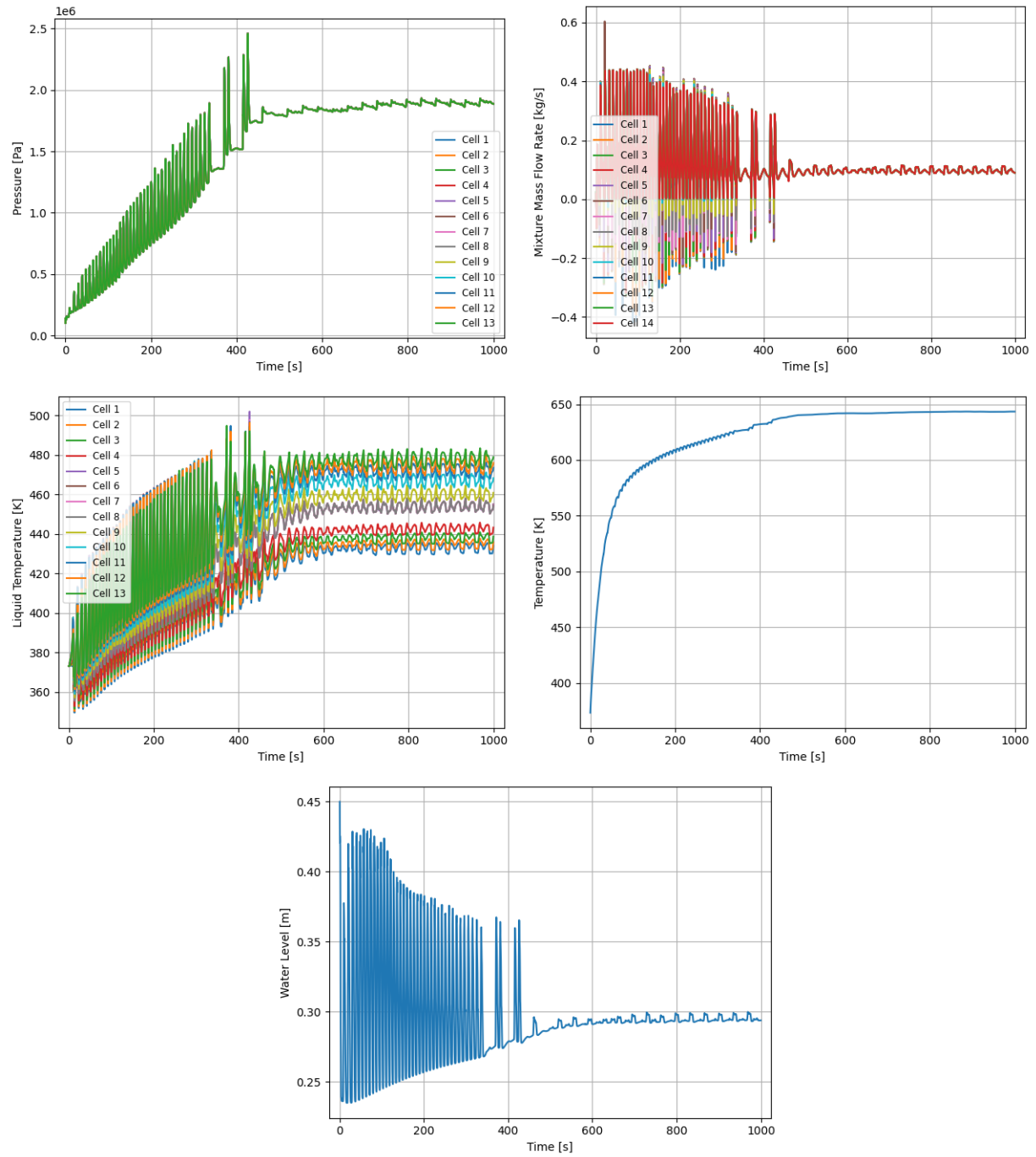


Figure 19. Pressurizer case with 97% initial liquid, including the target region pressure (top left), mass flow rate (top right), liquid temperature (mid left), and peak tungsten temperature (mid right), and pressurizer liquid level (bottom).

2.4 RESULTS WITH BELLOWS

An additional case was performed to assess the feasibility of using an expandable volume at the top of the loop, by means of a bellows or flexible bladder, for example, to allow the liquid in the loop to expand freely. This serves a similar function as the vapor volume at the top of the pressurizer: as a means of accommodating liquid density decrease as the liquid heats up, but the bellows concept would accomplish this purpose without any significant amount of vapor or gases within the closed loop.

TRACE does not have the ability to model volumes that change in size over time, which would be necessary to model this approach directly. However, a simplifying assumption was made that the bellows volume is infinitely flexible and expandable, with a negligible “spring” force or compressive force applied by the bellows onto the fluid.

Under these conditions, the pressure in the loop would remain fixed, equal to the pressure outside of the bellows. This allows the bellows to be modeled in TRACE simply as a fixed-pressure boundary condition, applied at the upper connector volume. Although the bellows region is not explicitly modeled in this approach, it will functionally behave the same in the TRACE simulation. (Fluid is allowed to flow from the loop into the implied bellows region, or vice versa.)

Note that atmospheric loop pressure could be achieved by exposing the bellows to ambient air; higher loop pressures could be achieved by encasing the bellows in a volume of air that is pressurized to a desired level. Alternatively, one could keep the bellows exposed to ambient air but account for the compressive force of the bellows onto the fluid, with the “stiffness” of the bellows chosen to achieve a desired loop pressure. The TRACE model, however, ignores such complexity and simply assumes a fixed pressure for this scoping study.

An initial case was run at 101.3 kPa (1 atm). At this pressure, the cooling ability of the fluid was insufficient to maintain acceptable target temperatures: runaway temperatures far exceeding 600 °C were observed and were caused by dryout and blanketing of the target channel surfaces with steam. Due to the infeasibility of that case, additional cases were run at higher loop pressures. A case at 2 MPa was attempted first because it approximates the pressure that was found to produce stable single-phase natural circulation in the pressurizer cases described above (Figure 19). As shown in Figure 20, this fixed pressure level resulted in stable behavior once again for the bellows case, with similar flow rates and temperatures as those observed in that case.

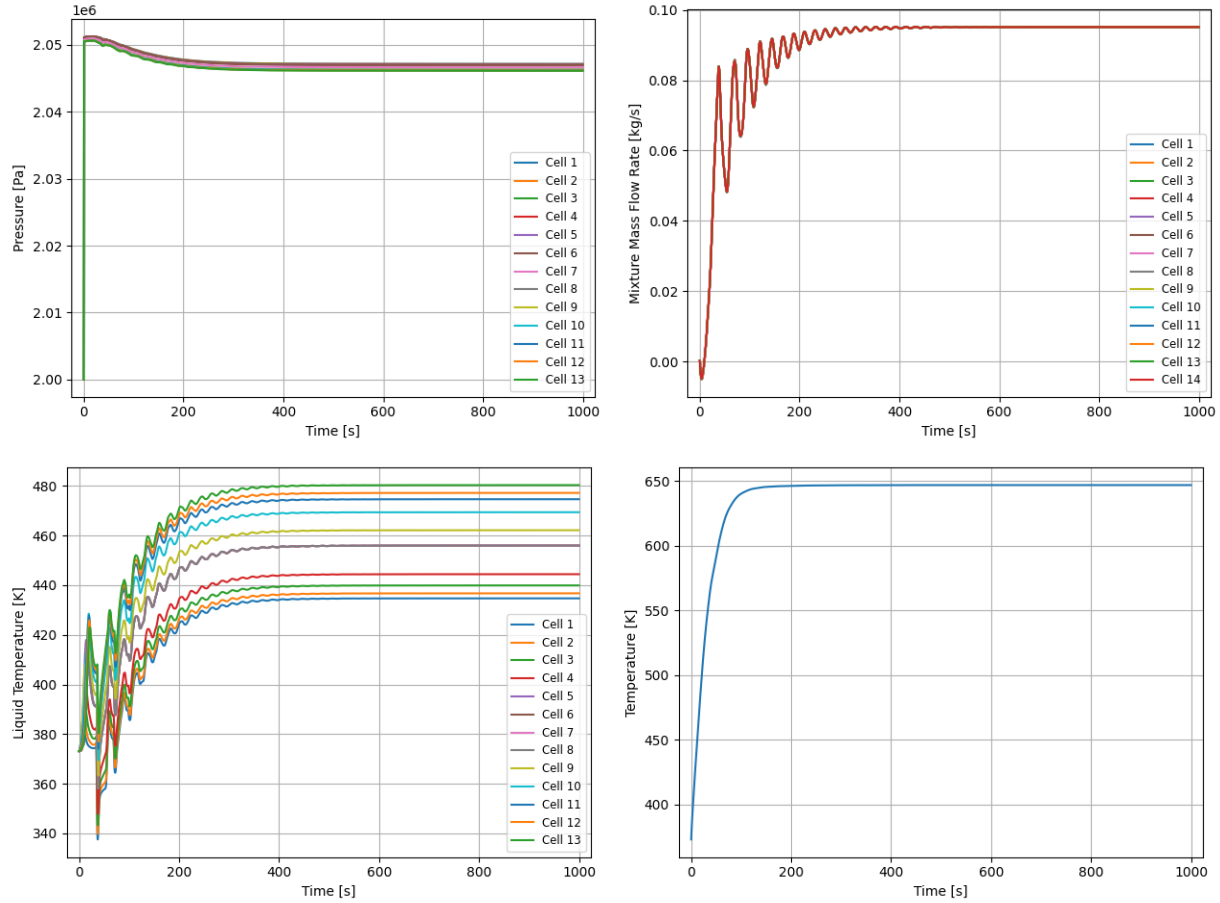


Figure 20. Bellows case results at 2 MPa, including the target region pressure (top left), mass flow rate (top right), liquid temperature (bottom left), and peak tungsten temperature (bottom right).

However, a fixed pressure of 1 MPa was found to produce oscillations, as shown in Figure 21. At this lower pressure, boiling occurred in the loop, which led to flow instability. Additional cases were run (not shown), and it was found that all cases above ~ 1.8 MPa were steady (i.e., non-oscillatory), and all cases below 1.8 MPa were oscillatory.

The same scenario was repeated with riser-to-condenser heat transfer added in (in addition to downcomer-to-condenser heat transfer). The results shown in Figure 21 and Figure 22 indicate that the system was stable for pressures of approximately 0.6 MPa and above; the improved condenser heat transfer allows the loop flow to remain single-phase while operating at these lower pressures.

Although the pressurizer case was not explicitly run with the riser-to-condenser heat transfer enabled, it is assumed that a similar stable operating condition near 0.6 MPa could be achieved using that approach as well, since the pressurizer and bellows approaches appear to behave similarly.

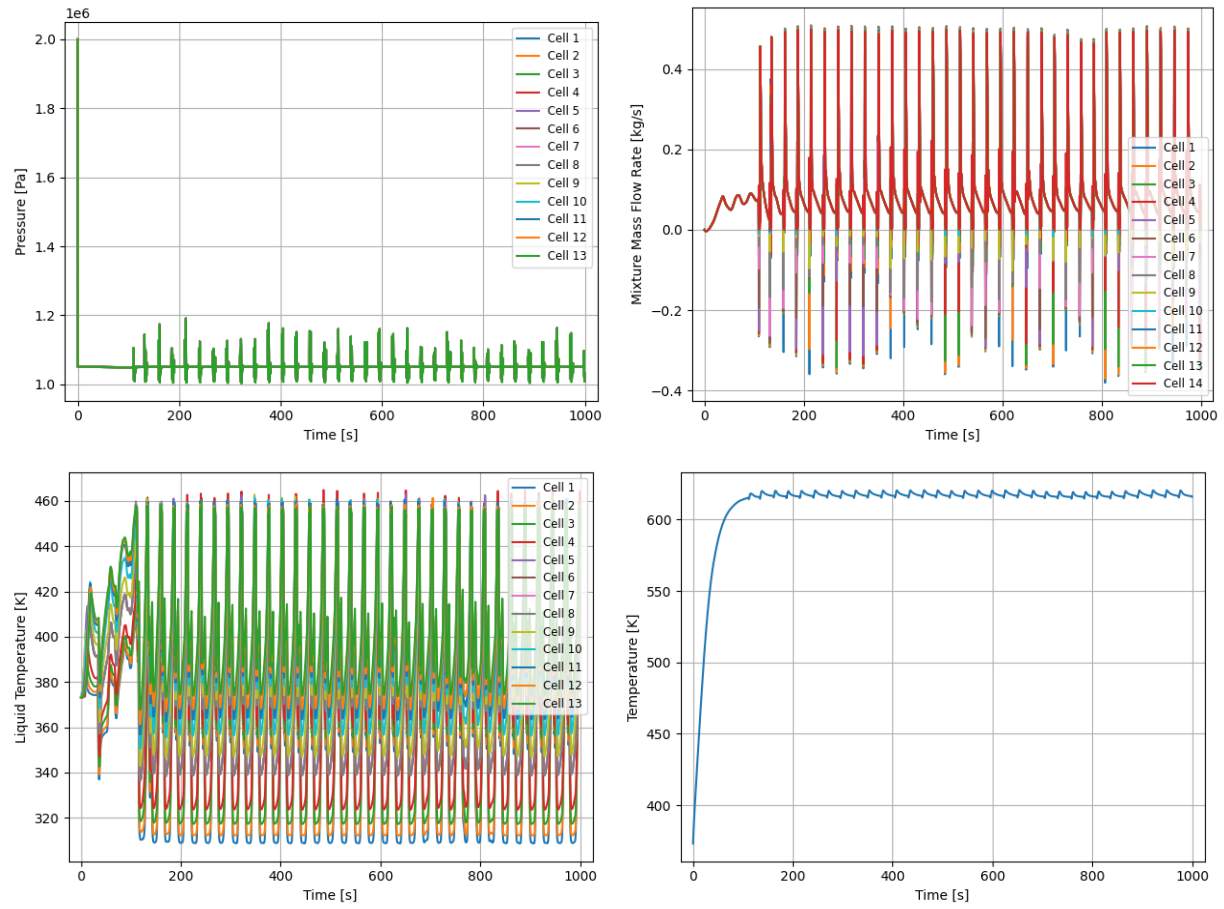


Figure 21. Bellows case results at 1 MPa, including the target region pressure (top left), mass flow rate (top right), liquid temperature (bottom left), and peak tungsten temperature (bottom right).

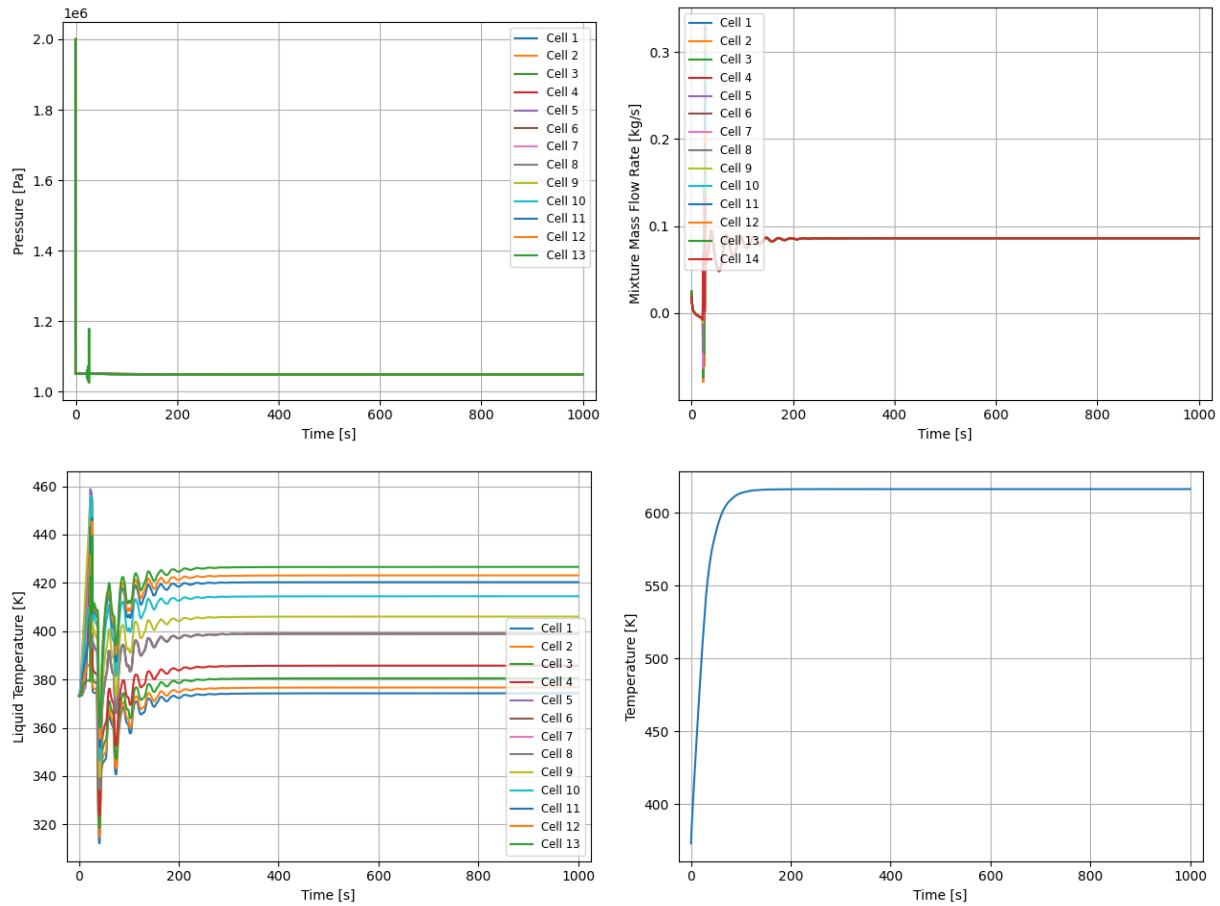


Figure 22. Bellows case results at 1 MPa after adding riser-to-condenser heat transfer; shown are the target region pressure (top left), mass flow rate (top right), liquid temperature (bottom left), and peak tungsten temperature (bottom right).

2.5 POSSIBLE ADDITIONAL DESIGN CHANGES TO CONSIDER

The following are additional design changes that could potentially improve the stability of the system. Note that based on further consideration, some of these changes may not be attainable based on existing design constraints but are mentioned here for completeness.

- Decreasing the loop friction losses, by decreasing form friction losses and/or increasing the hydraulic diameters of the flow path, promotes stability. Previous two-phase natural circulation experiments have found this to be the case [9, 10]. However, the loop may already have the largest hydraulic diameters and minimum form losses possible given the design constraints.
- Increasing the overall heat conductance (i.e., heat transfer capability) of the condenser by increasing the heated surface area or by other means will allow lower fluid temperatures and/or lower loop pressure at the given power level. This should allow for a lower vapor void fraction to be achieved while remaining in the desired pressure range, which should promote stability. This effect was observed when the riser-to-condenser heat transfer was added to the TRACE model

(Section 2.1 and 2.2) but should also be observable if the condenser length is increased beyond 0.75 m as well.

- Changing the overall height of the loop may impact stability. Increased height will increase the natural circulation driving head (increasing flow rates), but it could also increase the amount of void generation due to flashing (i.e., due to T_{sat} decreasing as elevation increases). Analysis would be required to determine whether increasing or decreasing the loop height would improve the stability.

3. REFERENCES

1. Bajorek, S.M., et al. 2015. *Development, validation and assessment of the TRACE thermal-hydraulics systems code*, in *NURETH-16*. Chicago, IL, U.S.A.
2. Duarte, J.P., et al. 2020. "Full-scale dryout/rewet instability tests in a BWR rod bundle and TRACE assessment." *Nuclear Engineering and Design* 370.
3. Kozlowski, T., et al. 2014. "Analysis of the OECD/NRC Oskarshamn-2 BWR stability benchmark." *Annals of Nuclear Energy* 67: 4-12.
4. Wysocki, A.J. 2015. *Investigation of limit cycle behavior in BWRs with time-domain analysis*. in *Nuclear Engineering and Radiological Sciences*. University of Michigan: Ann Arbor, Michigan.
5. *The Engineering Toolbox: Metals - Specific Heats*. 4/24/2023]. Available from: https://www.engineeringtoolbox.com/specific-heat-metals-d_152.html.
6. *Special Metals: Inconel Alloy 718*. 4/24/2023]. Available from: https://www.matweb.com/search/datasheet_print.aspx?matguid=94950a2d209040a09b89952d45086134.
7. *The Engineering Toolbox: Metals - Densities*. 4/24/2023]. Available from: https://www.engineeringtoolbox.com/metal-alloys-densities-d_50.html.
8. *The Engineering Toolbox: Metals, Metallic Elements and Alloys - Thermal Conductivities*. 4/24/2023]. Available from: https://www.engineeringtoolbox.com/thermal-conductivity-metals-d_858.html.
9. Nayak, A.K., et al. 2007. "Study on the stability behaviour of two-phase natural circulation systems using a four-equation drift flux model." *Nuclear Engineering and Design* 237(4): 386-398.
10. Vijayan, P.K., et al. 2008. "Effect of loop diameter on the steady state and stability behaviour of single-phase and two-phase natural circulation loops." *Science and Technology of Nuclear Installations* 2008: 17.

